Partial-wave analysis of K^+-nucleon scattering

John S. Hyslop, Richard A. Arndt, L. David Roper, and Ron L. Workman
*Department of Physics, Virginia Polytechnic Institute and State University, Blacksburg, Virginia 24061**
(Received 21 February 1992)

We have analyzed the available kaon-nucleon elastic-scattering data with laboratory kinetic energies below 2650 MeV. We present the results of an energy-dependent analysis and a set of energy-indepenedent analyses over this energy range. Our isoscalar amplitudes cover the region from threshold to 1100 MeV. The isovector amplitudes extend to 2650 MeV. Scattering lengths have been extracted. We also give pole positions and residues for resonancelike structures found in the P_{01}, D_{03}, P_{13}, and D_{15} partial waves. We compare our results to those from previous analyses.

PACS number(s): 13.75.Jz, 11.80.Et, 14.20.Jn

I. INTRODUCTION

The K^+-nucleon (K^+N) elastic reaction is interesting due to the possible presence of Z^* resonances [1,2]. One of the purposes of this work is to determine resonance pole positions for the isoscalar states in the K^+-nucleon reaction. No resonance pole positions are currently listed in the Particle Data Group Tables for the isoscalar states. Second, as it now seems likely that a kaon factory will be built at TRIUMF, a refinement of the K^+N amplitudes should be helpful in the planning of future experiments.

Hashimoto [2] has performed the most recent single-energy analysis of this system. Hashimoto included all reactions except elastic K^+-deuteron (K^+d) scattering data in his analysis, which covered values of $P_{\rm lab}$ from 0.6 to 1.5 GeV/c. Nakajima *et al.* [3] have carried out the most recent energy-dependent analysis of this system. Utilizing Alberi's [4] form factors and Martin's [5] energy-dependent parametrization, these authors also omitted elastic K^+d data in constructing their solution to 1.6 GeV/c. An earlier single-energy analysis was performed by Martin and Oades [6]. Here the set of single-energy solutions was smoothed by fixed-t dispersion relation constraints. This analysis included one set of the 1980s polarization data [7], but no K^+d elastic data.

Several studies of the isovector system exist. The energy-dependent analysis performed at Virginia Polytechnic Institute and State University (VPI&SU) is the most recent and extends up to 3 GeV/c [1]. The parametrization was based upon a two-channel coupled K matrix and guaranteed proper threshold behavior for the partial waves. Inelasticity was provided by the $K^+\Delta(1232)$ channel, except in the S_{11} partial wave where a K^*N coupling was assumed. Other analyses exist, but are older and have been superseded.

The present work is one of few simultaneous isoscalar and isovector analyses [2,3] of the K^+N scattering system since the polarization measurements [7–9] in the 1980s. The available K^+d elastic scattering data have also been analyzed. We have produced energy-dependent and energy-independent solutions which extend to a K^+ laboratory kinetic energy of 1100 MeV; the isovector amplitudes extend to 2650 MeV.

In Sec. II, we outline the database used in our analyses. Section III will briefly review the formalism used in describing the elastic scattering and deuteron-breakup reactions. In Sec. IV, the resulting partial-wave amplitudes will be displayed and compared with previous results. Finally, in Sec. V, we give our conclusions.

II. DATABASE

The K^+N reaction consists of two isospin states: $I=0$ (isoscalar) and $I=1$ (isovector). The isovector states have been determined, up to 2650 MeV, from the elastic K^+p reaction [1]. The current isovector database is discussed in Ref. [1]. Isoscalar states are determined from K^+d breakup and elastic reactions, and from K_L^0 scattering off a target proton. (Data acquired from these reactions actually contribute to both isoscalar and isovector states.) The deuteron is weakly bound and reactions can be described in an impulse approximation. This allows the neutron to be "extracted" as a target from the deuteron.

Table I displays a breakdown of the 1746 isoscalar data that have been considered in this analysis. The database consists of total ($\sigma_{\rm tot}$), elastic ($\sigma_{\rm el}$), inelastic ($\sigma_{\rm in}$), and differential ($\sigma(\theta)$) cross-section measurements. In addition, we have determinations (from forward dispersion relations) of the real part of the non-spin-flip forward scattering amplitude, Ref, as well as the existing polarization data. The range of incident lab kinetic energies and number of data within the range are denoted according to each experiment. The isoscalar contribution to the database is only sufficient below 1100 MeV. Above this energy, the data are too sparse to define these amplitudes.

The K^+d breakup reactions $K^+d\rightarrow K^+np$ and $K^+d\rightarrow K^0pp$ have been included in this analysis. These reactions have produced much of the data from which our isoscalar amplitudes have been determined. In addition to providing differential cross sections, the reactions

*Electronic mail address: phys0@vtcc1.bitnet.

TABLE I. Isoscalar K^+/N database ($T_{lab}=0-1100$ MeV).

Reaction	Observable	Energy (data)	Ref.
	Forward Data		
$K^+n\to K^+n$	σ_{tot}	522–1078(13)	[10]
$K^0_Lp\to K^+n$	σ_{el}	132(1)	[11]
$I=0$	σ_{tot}	149–680(19)	[12]
	σ_{in}	502–958(4)	[13]
		315–1095(13)	[14]
	Ref	39–1086(14)	[8]
	Angular data		
$K^+n\to K^+n$	$\sigma(\theta)$	621–1086(11)	[15]
	$P(\theta)$	490–945(43)	[5]
		675–1076(34)	[4]
$K^0_Lp\to K^+n$	$\sigma(\theta)$	303–555(9)	[16]
		322–1038(128)	[17]
$K^+n\to K^0p$	$P(\theta)$	283(5)	[18]
		490–945(39)	[6]
		675–1076(30)	[4]
$K^+d\to K^0pp$	$\sigma(\theta)$	100–456(26)	[19]
		283(10)	[18]
		502–958(80)	[20]
		314–1095(260)	[21]
		379–1095(116)	[22]
		163–564(114)	[23]
		60–273(40)	[24]
		354–524(60)	[25]
$K^+d\to K^+np$	$\sigma(\theta)$	127–231(10)	[26]
		314–1095(238)	[27]
		379–1010(75)	[28]
		163–564(99)	[23]
		107–273(29)	[24]
$K^+d\to K^+d$	$\sigma(\theta)$	314–1095(141)	[29]
		283–524(59)	[30]
		107–273(26)	[24]

$K^+d\to K^+np$ and $K^+d\to K^0pp$ have been used to deduce the K^+n elastic and charge-exchange reactions, as well as pure-isoscalar amplitudes.

III. K^+d FORMALISM

Single-scattering impulse approximations are used to describe the inelastic and elastic K^+d scattering. These approximations are justified [2] since the separation between the nucleons is relatively large in the deuteron, compared to the nucleon size. The interaction between the incident kaon and target nucleon is also weaker than in the case of pion-nucleon and nucleon-nucleon scattering. The relevant cross section formulas for these reactions are detailed in Ref. [2].

In the K^+d breakup reactions, one nucleon in the deuteron interacts with the scattering kaon; the remaining nucleon is considered a spectator. The outgoing spectator emerges with a momentum comparable with the Fermi momentum. Cutoffs for the spectator momenta arise from specifics of the experiment. Such measurements have generally been carried out in liquid-deuterium bubble chambers. In these chambers the visibility of the outgoing charged nucleon depends upon its momentum. The lower limit of visibility is approximately 100 MeV/c [27]. In $K^+d\to K^+np$ experiments the spectator is almost always the proton since this choice suppresses the K^+p amplitudes. The $K^+d\to K^+p\,(n)$ data (parentheses denote the spectator) are omitted since the two-body elastic K^+p data determine the elastic K^+p amplitudes much more accurately. The cutoffs for all K^+d breakup experiments ensure a low momentum transfer. A detailed discussion of cutoff values is given in Ref. [2].

In all of the $K^+d\to K^0p\,(p)$ experiments, a momentum constraint is placed on the spectator proton. Each of the nonspectator protons has a higher momentum than the spectator. The cross sections measured for this reaction have been scaled to an unconstrained cross section, which was measured either in the same or another experiment.

In order to determine the $K^+d\to K^+n\,(p)$ cross section, the $K^+d\to K^+p\,(n)$ and $K^+d\to K^+d$ contributions to the cross section must be removed from the measurement. Since the neutron is not detected, and the charge of the proton and deuteron are the same, this distinction is not trivial. The spectator is the proton and for the most part only K^+n amplitudes remain once the $K^+d\to K^+n\,(p)$ component is isolated.

Giacomelli *et al.* [27,28] make their measurement in a deuterium bubble chamber. In addition to placing limits on the proton momentum they scale to an unconstrained cross section. Our form-factor calculations verify that the choice of $p_{proton}<p_{neutron}$ effectively suppresses the K^+p amplitudes.

The Rutherford group [23] uses an "effective momentum cut" of 0 to 280 MeV/c in their selection of events. They detect the charged particle with scintillation counters and spark chambers. The means by which they remove K^+p amplitudes and the $K^+d\to K^+d$ contribution, beyond placing a momentum cut on the proton, is unclear. However, the data are for the most part consistent with the measurements of Giacomelli *et al.*

Glasser *et al.* [24] select all deuterium bubble-chamber events for which the spectator proton has momentum greater than 100 MeV/c [31]. Here, too, the means of removing $K^+p\to K^+p$ amplitudes is unclear. No scaling of their data is indicated, yet the magnitude of their cross sections is consistent with other unconstrained cross sections. A hump, which disagrees with the Rutherford data [23], arises at one energy in this data set.

Adams *et al.* [15] report measurements of K^+n elastic cross sections at 180° from a measurement of $K^+d\to K^+n\,(p)$. They do not describe the technique by which the elastic cross sections are acquired, yet the general magnitude of the cross sections is consistent with the extrapolated values from other [27,28] measurements.

Stenger *et al.* [26] measure a combination of $K^+d\to K^+np$ and $K^+d\to K^+d$ cross-section data. The $K^+d\to K^+d$ contribution is shown to be small and the data are fitted as $K^+d\to K^+np$ with no spectator momentum cuts.

We have chosen to represent the K^+d elastic reaction by a single scattering process since this is a reasonable approximation, given the large errors on the differential cross-section data. Formulas for the differential cross

sections are given in Refs. [29] and [35]. According to plots of $\sigma(\theta)$ from Hashimoto [32] at $p_L \geq 900$ MeV/c, many of the single-scattering contributions fall within or slightly outside the errors, where data exist, at forward angles. Ferreira [33] estimates the effect of multiple scattering in the impulse approximation at $T_L = 100$ MeV to be less than 10% for the cross sections. In a calculation by Garcilazo [34], the Faddeev calculation improves on the impulse approximation only for differential cross section data with $p_{\rm lab} \leq 587$ MeV/c and $\theta_{\rm lab} \geq 70°$. The region in question contains only eleven measurements, or about 5% of the $K^+d \to K^+d$ database. The Faddeev calculation [34] and the results of Hashiomoto [32] depart in their predictions of differential cross sections mainly in regions where no data exist.

IV. THE PARTIAL-WAVE AMPLITUDES

The partial-wave analysis couples two complementary techniques of analysis. The first technique, the single-energy or energy-independent analysis, assumes linearity of the phases and absorption parameters within a small energy bin of data. The second technique, the energy-dependent analysis, provides a smooth solution over the entire kinematic range, perhaps missing some small structures. The energy-dependent parametrization utilizes a coupled-channel K matrix. The inelasticities of the isovector and isoscalar channels are provided by the $K^+\Delta(1232)$ and $K^+{}^*(892)N$ states, respectively; a $K^+{}^*(892)N$ coupling is used for the S_{11} partial wave. These two techniques are used iteratively to ensure that the energy-dependent solution contains those structures suggested by the single-energy results. The final single-energy solutions are useful to indicate the accuracy of a solution. All solutions are obtained through χ^2 minimization on a renormalizable database.

Our results are extensions of a previous analysis [1] of K^+p data to 3 GeV. The isovector amplitudes from Ref. [1] served as a starting point for the present analysis. The representation was made more economical through a reduction in the number of varied parameters from 75 to

TABLE II. Energy range and χ^2/datum for single-energy solutions. The corresponding χ^2/datum values for SP92 and the isoscalar data are given, as well as the number of parameters (N_p) used in the fit.

$T_{\rm lab}$ (range) (MeV)		χ^2datum ($I=0$)	N_p	χ^2(SP92)
75(50–100)	169/107	59/17	1	176
150(125–175)	76/67	42/35	6	81
200(175–225)	109/71	74/36	7	131
250(225–275)	244/100	213/71	7	307
300(275–325)	275/194	196/133	7	327
350(325–375)	164/112	113/73	7	192
400(375–425)	300/188	182/125	8	346
450(425–475)	216/151	154/106	8	234
500(475–525)	397/314	256/192	11	420
550(525–575)	258/242	138/105	12	281
600(575–625)	213/215	149/122	14	235
700(675–725)	227/213	152/117	16	295
750(720–780)	240/193	136/80	17	275
820(780–860)	321/286	132/124	22	396
900(850–950)	530/400	379/213	24	599
1025(950–1100)	739/618	281/218	24	808
1100(1050–1150)	245/249		15	318
1200(1150–1250)	317/312		16	392
1300(1250–1350)	405/292		16	452
1400(1350–1450)	378/263		16	397
1500(1450–1550)	308/249		18	350
1650(1600–1700)	405/246		18	460
1800(1700–1900)	82/87		18	113
2000(1900–2100)	194/181		20	238
2200(2100–2300)	145/105		20	187
2500(2300–2700)	107/93		20	193

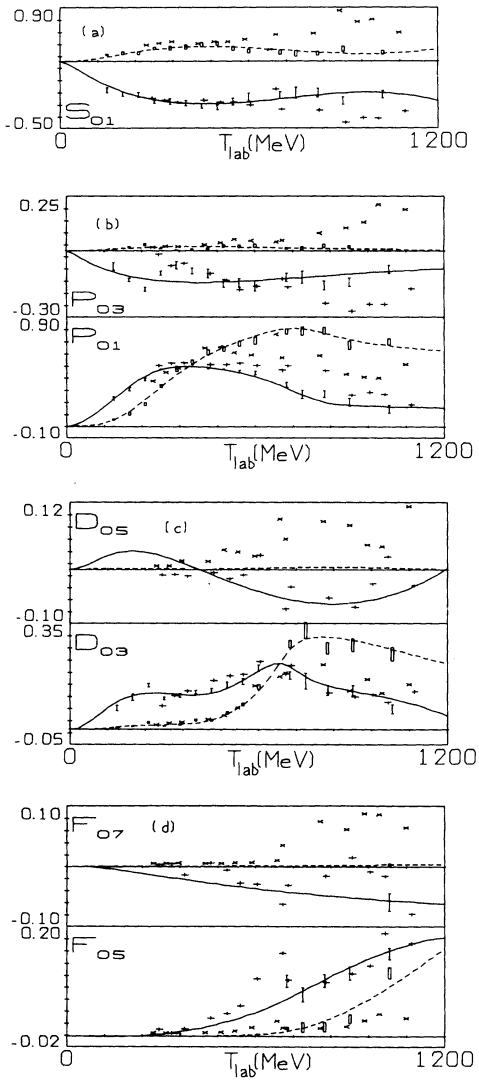

FIG. 1. Isoscalar T-matrix values versus $T_{\rm lab}$ for solution SP92. The real (imaginary) parts are represented as solid (dashed) lines. The bars and boxes represent our single-energy solutions. The (+) and (×) symbols denote the single-energy results of Hashimoto [2]. (a) S_{01}, (b) P_{03} and P_{01}, (c) D_{05} and D_{03}, (d) F_{07} and F_{05}.

62. This resulted in a χ^2 increase of about 100 for the 3663 K^+p data below $T_{\rm lab}=2650$ MeV. Two different techniques were used to find isoscalar energy-dependent solutions up to an incident lab kinetic energy of 1100 MeV. The first technique involved initializing to the single-energy solutions of Hashimoto [2], and Martin and Oades [9]. The use of two single-energy solutions guaranteed independent starting points as they differed greatly. The second technique involved incrementally increasing the range of the energy-dependent fit while also increasing the number of fitted partial waves. All techniques gave very similar results for the isoscalar partial waves. The best fit was adopted as the starting point for a combined data fit with both $I=1$ and $I=0$ waves being searched. The resulting solution, which we denote as SP92, is summarized as follows. In addition to the 62 parameters used to fit the isovector partial waves, 29 parameters were searched for the isoscalar waves. The isovector result, extending to 2650 MeV, required the inclusion of 15 partial waves, up to $L=7$. The isoscalar waves, which extend to 1100 MeV, require the inclusion of 9 partial waves, up to $L=4$. The 3663 K^+p elastic scattering data were fitted with a χ^2 of 4875. The remaining database of 1746 measurements, contributing mainly to the isoscalar solution, was fitted with a χ^2 of 3181. The single-energy fits to binned data are compared with SP92 in Table II. The difference in χ^2 between the single-energy fits and SP92 is quite reasonable.

Plots of the real and imaginary parts of the T matrix, versus the K^+ lab kinetic energy, are given in Figs. 1 and 2. Single-energy results are also plotted for comparison. (Single-energy solutions were not determined for the very small D_{05} partial wave, and at only one energy for the F_{07} wave.) The real and imaginary parts of the T matrix are given in terms of δ and η by $(\eta\sin2\delta)/2$ and $(1-\eta\cos2\delta)/2$, respectively. Values of δ and η are given in Table III. In the isoscalar solution, the $L=J-\frac{1}{2}$ real partial-wave amplitudes are negative, while the waves with $L=J+\frac{1}{2}$ are positive. Since the sign of the ReT indicates the sign of the phase shift, the $L=J-\frac{1}{2}$ partial-wave amplitudes suggest repulsive potential effects and, for the $L=J+\frac{1}{2}$ amplitudes, attraction. This isoscalar trend of attractiveness and repulsiveness agrees with the

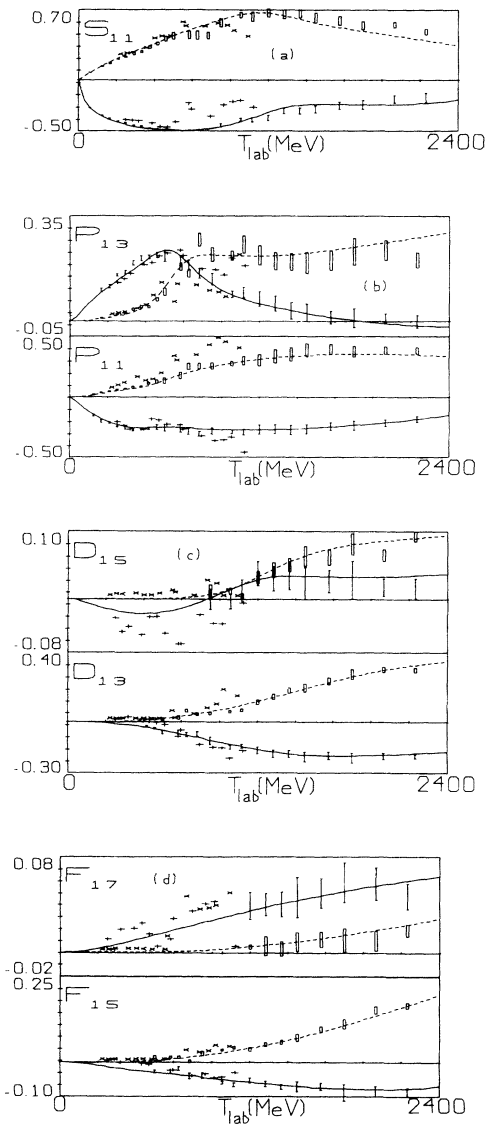

FIG. 2. Isovector T-matrix values. Notation as in Fig. 1. (a) S_{11}, (b) P_{13} and P_{11}, (c) D_{15} and D_{13}, (d) F_{17} and F_{15}.

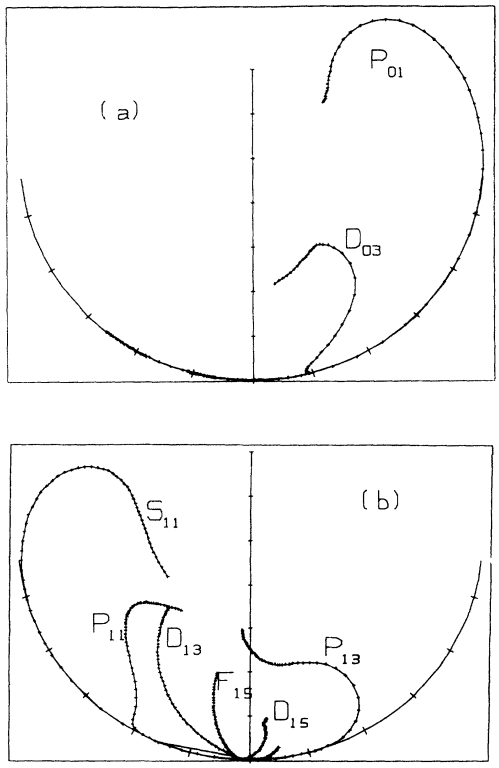

FIG. 3. Argand diagrams. (a) Isoscalar partial waves, (b) isovector partial waves. The hash marks are separated by 50 MeV increments in $T_{\rm lab}$.

TABLE III. Partial-wave amplitudes listed as $(\delta, 1-\eta^2)$ pairs. See text for definitions. Values of δ are given in degrees.

(a)

T_{lab} (MeV)	S_{01}		S_{11}		T_{lab} (MeV)	S_{01}		S_{11}	
50.0	−3.13	0.000	−13.35	0.000	600.0	−18.56	0.000	−41.15	0.013
100.0	−6.98	0.000	−18.40	0.000	650.0	−17.81	0.000	−42.74	0.021
150.0	−10.43	0.000	−22.09	0.000	700.0	−16.96	0.000	−44.28	0.031
200.0	−13.30	0.000	−25.11	0.000	750.0	−16.08	0.000	−45.79	0.043
250.0	−15.58	0.000	−27.72	0.000	800.0	−15.25	0.000	−47.26	0.059
300.0	−17.29	0.000	−30.07	0.000	850.0	−14.53	0.000	−48.69	0.078
350.0	−18.49	0.000	−32.21	0.000	900.0	−13.99	0.000	−50.08	0.102
400.0	−19.22	0.000	−34.20	0.000	950.0	−13.69	0.000	−51.43	0.131
450.0	−19.53	0.000	−36.07	0.001	1000.0	−13.69	0.000	−52.71	0.164
500.0	−19.48	0.000	−37.83	0.003	1050.0	−14.05	0.000	−53.92	0.203
550.0	−19.14	0.000	−39.52	0.007	1100.0	−14.81	0.000	−55.03	0.246

(b)

T_{lab} (MeV)	P_{01}		P_{03}		P_{11}		P_{13}	
50.0	2.24	0.000	−1.96	0.000	−2.55	0.000	1.21	0.000
100.0	6.99	0.000	−3.97	0.000	−5.46	0.000	2.76	0.000
150.0	13.41	0.000	−5.50	0.000	−7.99	0.000	4.23	0.000
200.0	20.67	0.000	−6.58	0.000	−10.11	0.000	5.55	0.000
250.0	28.00	0.000	−7.33	0.000	−11.87	0.000	6.74	0.000
300.0	34.79	0.002	−7.80	0.000	−13.30	0.003	7.85	0.001
350.0	40.77	0.005	−8.08	0.000	−14.40	0.008	8.94	0.002
400.0	45.88	0.010	−8.19	0.000	−15.18	0.021	10.06	0.006
450.0	50.23	0.018	−8.18	0.000	−15.67	0.049	11.29	0.017
500.0	53.99	0.029	−8.08	0.000	−15.99	0.099	12.69	0.043
550.0	57.35	0.047	−7.91	0.000	−16.42	0.169	14.25	0.094
600.0	60.51	0.074	−7.69	0.000	−17.14	0.242	15.77	0.180
650.0	63.69	0.122	−7.43	0.000	−18.12	0.306	16.90	0.293
700.0	66.99	0.210	−7.15	0.000	−19.24	0.357	17.20	0.410
750.0	69.84	0.349	−6.86	0.000	−20.39	0.398	16.54	0.506
800.0	71.39	0.495	−6.56	0.000	−21.50	0.430	15.17	0.571
850.0	71.58	0.608	−6.26	0.000	−22.54	0.457	13.52	0.609
900.0	70.84	0.684	−5.97	0.000	−23.51	0.479	11.92	0.631
950.0	69.67	0.734	−5.68	0.000	−24.39	0.499	10.50	0.642
1000.0	68.40	0.768	−5.42	0.000	−25.19	0.517	9.30	0.649
1050.0	67.21	0.792	−5.17	0.000	−25.92	0.533	8.28	0.653
1100.0	66.16	0.811	−4.95	0.000	−26.57	0.548	7.41	0.657

(c)

T_{lab} (MeV)	D_{03}		D_{05}		D_{13}		D_{15}	
50.0	0.96	0.000	0.37	0.000	−0.01	0.000	−0.07	0.000
100.0	3.19	0.000	1.11	0.000	−0.05	0.000	−0.25	0.000
150.0	5.26	0.000	1.66	0.000	−0.15	0.000	−0.47	0.000
200.0	6.55	0.000	1.84	0.000	−0.30	0.000	−0.68	0.000
250.0	7.05	0.001	1.70	0.000	−0.50	0.000	−0.87	0.000
300.0	7.02	0.004	1.31	0.000	−0.74	0.001	−1.02	0.000
350.0	6.81	0.013	0.76	0.000	−1.01	0.002	−1.13	0.000
400.0	6.77	0.030	0.12	0.000	−1.30	0.006	−1.21	0.000
450.0	7.22	0.062	−0.55	0.000	−1.61	0.015	−1.25	0.000
500.0	8.43	0.114	−1.20	0.000	−1.99	0.028	−1.24	0.000
550.0	10.58	0.189	−1.82	0.000	−2.45	0.043	−1.20	0.001
600.0	13.72	0.290	−2.37	0.000	−2.98	0.058	−1.13	0.002
650.0	17.67	0.427	−2.84	0.000	−3.55	0.074	−1.01	0.003
700.0	20.83	0.600	−3.22	0.000	−4.16	0.091	−0.86	0.005
750.0	20.62	0.713	−3.48	0.000	−4.80	0.109	−0.67	0.008
800.0	19.15	0.755	−3.63	0.000	−5.47	0.128	−0.45	0.012

TABLE III. (*Continued*).

850.0	17.62	0.767	−3.66	0.000	−6.17	0.148	−0.20	0.018
900.0	16.09	0.765	−3.56	0.000	−6.88	0.169	0.07	0.027
950.0	14.47	0.757	−3.32	0.000	−7.62	0.191	0.37	0.037
1000.0	12.74	0.744	−2.94	0.000	−8.37	0.214	0.67	0.050
1050.0	10.89	0.728	−2.42	0.000	−9.14	0.238	0.98	0.066
1100.0	8.93	0.711	−1.75	0.000	−9.92	0.263	1.27	0.084

(d)

T_{lab} (MeV)	F_{05}		F_{07}		F_{15}		F_{17}	
50.0	−0.01	0.000	−0.02	0.000	−0.01	0.000	0.00	0.000
100.0	−0.03	0.000	−0.11	0.000	−0.09	0.000	0.03	0.000
150.0	−0.04	0.000	−0.27	0.000	−0.23	0.000	0.07	0.000
200.0	−0.01	0.000	−0.47	0.000	−0.40	0.000	0.13	0.000
250.0	0.08	0.000	−0.70	0.000	−0.58	0.000	0.20	0.000
300.0	0.22	0.000	−0.92	0.000	−0.77	0.000	0.28	0.000
350.0	0.43	0.000	−1.14	0.000	−0.95	0.000	0.36	0.000
400.0	0.70	0.000	−1.36	0.000	−1.11	0.001	0.45	0.000
450.0	1.04	0.001	−1.56	0.000	−1.26	0.003	0.55	0.000
500.0	1.45	0.002	−1.76	0.000	−1.39	0.006	0.64	0.000
550.0	1.94	0.003	−1.94	0.000	−1.52	0.011	0.74	0.000
600.0	2.52	0.006	−2.11	0.000	−1.66	0.018	0.83	0.001
650.0	3.19	0.010	−2.27	0.000	−1.80	0.025	0.93	0.001
700.0	3.99	0.018	−2.43	0.000	−1.95	0.033	1.03	0.002
750.0	4.90	0.033	−2.57	0.000	−2.10	0.042	1.13	0.002
800.0	5.87	0.057	−2.71	0.000	−2.26	0.051	1.23	0.003
850.0	6.87	0.087	−2.83	0.000	−2.41	0.061	1.33	0.004
900.0	7.90	0.124	−2.95	0.000	−2.57	0.071	1.43	0.005
950.0	8.93	0.165	−3.07	0.000	−2.73	0.082	1.53	0.006
1000.0	9.97	0.210	−3.17	0.000	−2.89	0.094	1.62	0.007
1050.0	11.00	0.257	−3.28	0.000	−3.05	0.106	1.72	0.009
1100.0	12.02	0.306	−3.37	0.000	−3.22	0.119	1.81	0.010

(e)

T_{lab} (MeV)	G_{07}		G_{09}		G_{17}		G_{19}	
50.0	0.01	0.000	0.00	0.000	0.00	0.000	0.00	0.000
100.0	0.08	0.000	−0.02	0.000	0.02	0.000	0.00	0.000
150.0	0.24	0.000	−0.05	0.000	0.07	0.000	0.00	0.000
200.0	0.42	0.000	−0.10	0.000	0.13	0.000	0.00	0.000
250.0	0.59	0.000	−0.17	0.000	0.19	0.000	0.00	0.000
300.0	0.71	0.000	−0.24	0.000	0.24	0.000	0.00	0.000
350.0	0.77	0.000	−0.32	0.000	0.29	0.000	0.01	0.000
400.0	0.75	0.001	−0.40	0.000	0.32	0.000	0.01	0.000
450.0	0.69	0.001	−0.48	0.000	0.33	0.001	0.02	0.000
500.0	0.58	0.002	−0.56	0.000	0.33	0.003	0.03	0.000
550.0	0.45	0.004	−0.63	0.000	0.30	0.005	0.05	0.000
600.0	0.33	0.007	−0.70	0.000	0.25	0.007	0.06	0.000
650.0	0.23	0.011	−0.77	0.000	0.18	0.010	0.08	0.000
700.0	0.20	0.018	−0.84	0.000	0.08	0.012	0.10	0.000
750.0	0.25	0.029	−0.90	0.000	−0.03	0.015	0.12	0.000
800.0	0.40	0.048	−0.96	0.000	−0.16	0.018	0.14	0.000
850.0	0.63	0.076	−1.02	0.000	−0.29	0.020	0.17	0.000
900.0	0.94	0.114	−1.08	0.000	−0.44	0.023	0.19	0.000
950.0	1.30	0.161	−1.13	0.000	−0.60	0.026	0.21	0.000
1000.0	1.70	0.217	−1.18	0.000	−0.77	0.030	0.24	0.000
1050.0	2.11	0.281	−1.23	0.000	−0.95	0.034	0.27	0.000
1100.0	2.53	0.350	−1.27	0.000	−1.13	0.038	0.29	0.000

TABLE IV. Pole positions and residues from the energy-dependent solution SP92.

Amplitude	Result	Position (MeV) ReW	Position (MeV) $-$ImW	Residue (MeV) (modulus)
P_{01}	Pole	1831	95	25
D_{03}	Pole	1788	170	42
P_{13}	Pole	1811	118	19
D_{15}	Pole	2074	253	16

single-energy solutions of Hashimoto, and Martin and Oades, with the exception of the G_{09} wave of Martin and Oades.

A. Resonance poles

Poles are associated with each of the partial-wave amplitudes that display a counterclockwise looping behavior in the Argand diagram. These partial waves are the P_{01}, D_{03}, P_{13}, and D_{15}. Argand plots are displayed in Fig. 3. The above poles are also evident in Fig. 4, where we have contour plotted the complex energy plane. The locations

TABLE V. Previous pole predictions and determinations for Z^* resonances. The Z^* subscript denotes the isospin.

	Z_1^* (GeV)	Z_0^* (GeV)
S_1	1.78 [38]	1.71 [38]
	2.2–2.25 [40]	1.95 [40]
	1.89, 2.13	1.70
P_1	1.9	1.72
		1.778 [3]
P_3	1.9	1.72
	1.931 [3]	
D_3	1.80, 2.16	1.99
		1.907 [3]
D_5	2.16	
F_5	1.9	

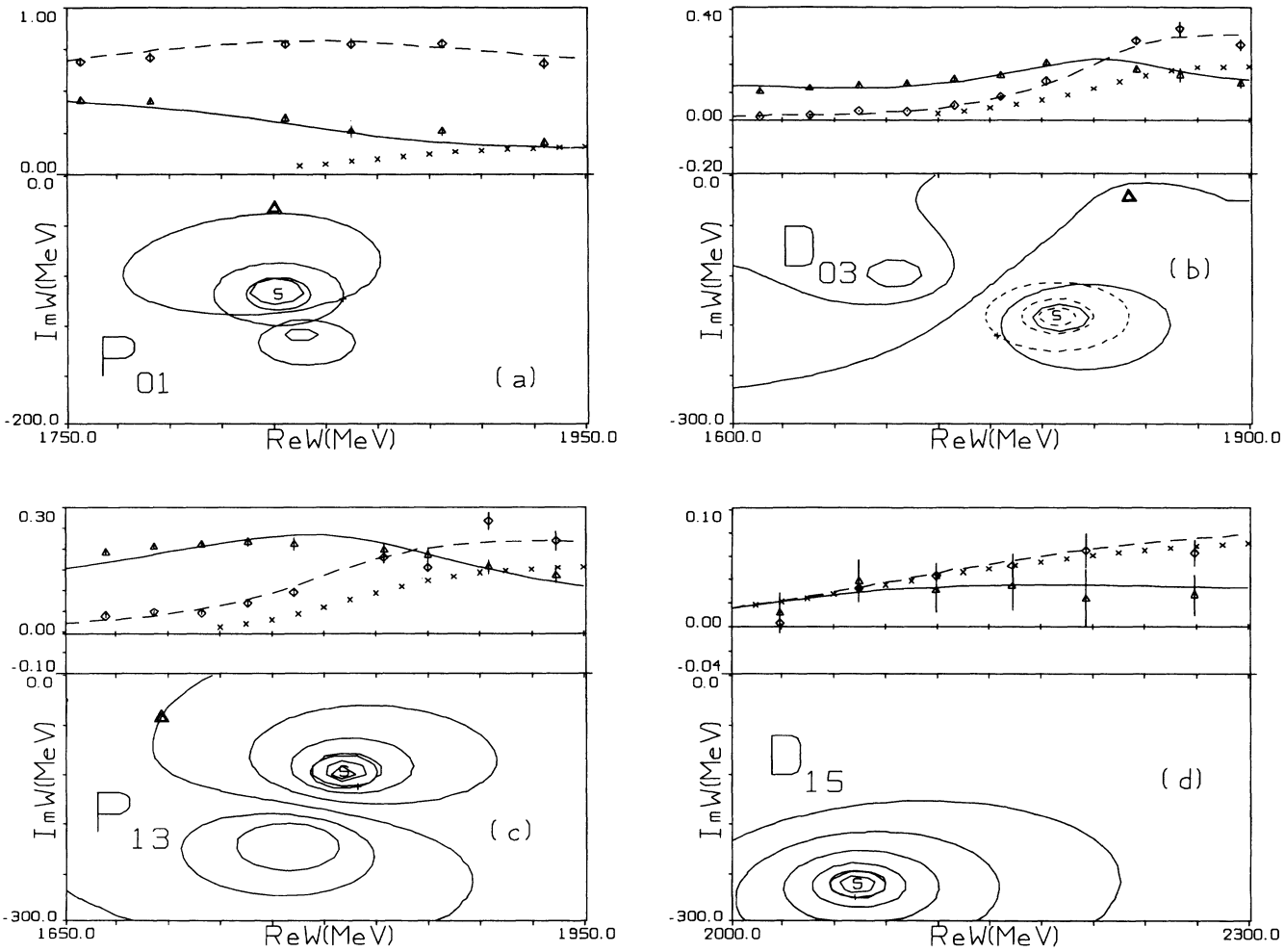

FIG. 4. Amplitude and complex plane plots for the solution SP92. The real (imaginary) part of the T matrix is plotted as a full (dashed) curve with single-energy values denotes by triangles (diamonds). The value of $\mathrm{Im}T - |T|^2$ is indicated by the $\times$. Contours are plotted for $|T|^2$. S denotes a pole position. The other extrema in these plots are zeros. Δ indicates the branch point (a) P_{01}, (b) D_{03}, (c) P_{13}, (d) D_{15}.

TABLE VI. Scattering lengths and volumes from SP92 and previous analyses.

	a_{0_+} (fm)		a_{1_-} (fm^3)		a_{1_+} (fm^3)	
	$I=1$	$I=0$	$I=1$	$I=0$	$I=1$	$I=0$
SP92	−0.33	0.0	−0.16	0.08	0.07	−0.13
Analysis I [42]	−0.28		−0.038		0.019	
Analysis II [43]	−0.33	0.02				
Analysis III [5]	−0.32	−0.035	−0.032	0.086	0.021	−0.019

of the poles and their residues are tabulated in Table IV.

Theoretical predictions [36–40] for pole positions also exist. Resonance mass predictions are listed in Table V.

B. Scattering lengths

Previous partial-wave analyses [41] have calculated isoscalar and isovector scattering lengths, which can be compared with this analysis. The scattering lengths for the present analysis were acquired by extending the energy-dependent solution to an incident momentum of 10 MeV and approximating its value at threshold. As a result, no errors are provided. Values are listed in Table VI.

V. CONCLUSIONS

The isoscalar states in the K^+N scattering reaction appear to follow a trend. The $j=l-\frac{1}{2}$ states suggest an attractive potential effect while the $j=1+\frac{1}{2}$ show repulsion. Buttgen *et al.* [44] predict this trend within their meson exchange model.

Broad motion in the counterclockwise direction is recorded in the P_{01}, D_{03}, P_{13}, and D_{15} Argand diagrams. Resonance poles are found for each of these partial waves, the D_{03} pole appearing on the second sheet.

The isoscalar and isovector scattering lengths, which we have determined, are quite consistent with previous determinations. The isoscalar scattering length was found to be compatible with zero. Predictions of these analyses can be obtained interactively through the SAID program [45] or from the authors upon request.

ACKNOWLEDGMENTS

This work was supported in part by the U. S. Department of Energy Grant No. DE-AS05-76ER04928.

[1] R. A. Arndt and L. D. Roper, Phys. Rev. D **31**, 2230 (1985).
[2] K. Hashimoto, Phys. Rev. C **29**, 1377 (1984).
[3] K. Nakajima *et al.*, Phys. Lett. **112B**, 80 (1982).
[4] G. Alberi *et al.*, Istituto Nazionale di Fisica Nucleare Report No. INFN/AE-72/3, 1972 (unpublished).
[5] B. R. Martin, Nucl. Phys. **B94**, 413 (1975).
[6] B. R. Martin and G. C. Oades, in *Baryon 1980,* Proceedings of the IVth International Conference of Baryon Resonances, Toronto, edited by N. Isgur (University of Toronto Press, Toronto, 1981).
[7] A. W. Robertson *et al.*, Phys. Lett. **91B**, 465 (1980).
[8] K. Nakajima *et al.*, Phys. Lett. **112B**, 75 (1982).
[9] S. J. Watts *et al.*, Phys. Lett. **95B**, 323 (1980).
[10] R. L. Cool *et al.*, Phys. Rev. D **1**, 1887 (1970).
[11] G. W. Meisner and F. S. Crawford, Phys. Rev. D **3**, 2553 (1971).
[12] A. S. Carroll *et al.*, Phys. Lett. **45B**, 531 (1973).
[13] A. A. Hirata *et al.*, Nucl. Phys. **B33**, 525 (1971).
[14] G. Giacomelli *et al.*, Nucl. Phys. **B37**, 577 (1972).
[15] U. Adams *et al.*, Nucl. Phys. **B87**, 41 (1975).
[16] R. M. Edelstein *et al.*, Phys. Rev. D **14**, 702 (1976).
[17] J. C. M. Armitage *et al.*, Nucl. Phys. **B123**, 11 (1977).
[18] A. K. Ray *et al.*, Phys. Rev. **183**, 1183 (1969).
[19] W. Slater *et al.*, Phys. Rev. Lett. **7**, 378 (1961).
[20] A. A. Hirata *et al.*, Nucl. Phys. **B30**, 157 (1971).
[21] G. Giacomelli *et al.*, Nucl. Phys. **B42**, 437 (1972).
[22] P. Lugaresi-Serra *et al.*, Istituto Nazionale di Fisica Nucleare Report No. INFN/AE-73/9, 1973 (unpublished).
[23] C. J. S. Damerell *et al.*, Nucl. Phys. **B94**, 374 (1975).
[24] R. G. Glasser *et al.*, Phys. Rev. D **15**, 1200 (1977).
[25] M. Sakitt, J. Skelly, and J. Thompson, Phys. Rev. D **15**, 1846 (1977).
[26] V. J. Stenger *et al.*, Phys. Rev. **134**, B1111 (1964).
[27] G. Giacomelli *et al.*, Nucl. Phys. **B56**, 346 (1973).
[28] G. Giacomelli *et al.*, Istituto Nazionale di Fisica Nucleare Report No. INFN/AE-73/4, 1973 (unpublished).
[29] G. Giacomelli *et al.*, Nucl. Phys. **B68**, 285 (1974).
[30] M. Sakitt, J. Skelly, and J. A. Thompson, Phys. Rev. D **12**, 3386 (1975).
[31] G. Snow (private communication).
[32] K. Hashimoto, dissertation, Department of Nuclear Engineering, Kyoto University, Japan, 1983.
[33] E. M. Ferreira, Phys. Rev. **115**, 1727 (1959).
[34] H. Garcilazo, Phys. Rev. C **37**, 2022 (1988).
[35] K. Hashimoto, Phys. Rev. C **27**, 1572 (1983).
[36] J. J. de Swart, P. J. Mulders, and L. J. Somers, in *Baryon 1980* [6].
[37] T. DeGrand, R. L. Jaffe, K. Johnson, and J. Kiskis, Phys. Rev. D **12**, 2060 (1975).
[38] C. Roiesnol, Phys. Rev. D **20**, 1646 (1979).
[39] R. J. Jaffe and F. E. Low, Phys. Rev. D **19**, 2105 (1979).
[40] Earle L. Lomon, in *Proceedings of the 8th International Symposium on High Energy Spin Physics,* Minneapolis, Minnesota, 1988, edited by K. Heller, AIP Conf. Proc. No. 187 (AIP, New York, 1988).

[41] Carl B. Dover and George E. Walker, Phys. Rep. **89**, 1 (1982).
[42] R. E. Cutkosky *et al.*, Nucl. Phys. **B102**, 139 (1976).
[43] A. D. Martin, Phys. Lett. **65B**, 346 (1976).
[44] R. Büttgen, K. Holinde, and J. Speth, Phys. Lett. **163B**, 305 (1985); Nuovo Cimento **102**, 247 (1989).
[45] The Scattering Analysis Interactive Dial-in program is available through Telnet: VTINTE.PHYS.VT.EDU or 128.173.7.3. The logon/password is PHYSICS/QUANTUM. Users can compare different solutions and access the database used in the present analysis.